AGU PUBLICATIONS

JGR

Journal of Geophysical Research: Space Physics

RESEARCH ARTICLE
10.1002/2017JA024826

Bow Shock Generator Current Systems: MMS Observations of Possible Current Closure

M. Hamrin[1], H. Gunell[1,2], J. Lindkvist[1], P.-A. Lindqvist[3], R. E. Ergun[4], and B. L. Giles[5]

[1]Department of Physics, Umeå University, Umeå, Sweden, [2]Belgian Institute for Space Aeronomy, Brussels, Belgium, [3]Royal Institute of Technology, Stockholm, Sweden, [4]Laboratory of Atmospheric and Space Physics, Boulder, CO, USA, [5]NASA Goddard Space Flight Center, Greenbelt, MD, USA

Key Points:
- These are the first observations of bow shock current closure across the magnetosheath and toward the magnetosphere
- For large IMF $|B_z|$, there are indications of current closure in the equatorial plane
- For large IMF $|B_y|$, the current system is tilted and closure may occur at higher latitudes

Correspondence to:
M. Hamrin,
hamrin@space.umu.se

Citation:
Hamrin, M., Gunell, H., Lindkvist, J., Lindqvist, P.-A., Ergun, R. E., & Giles, B. L. (2018). Bow shock generator current systems: MMS observations of possible current closure. *Journal of Geophysical Research: Space Physics*, *123*, 242–258. https://doi.org/10.1002/2017JA024826

Received 28 SEP 2017
Accepted 28 NOV 2017
Accepted article online 6 DEC 2017
Published online 10 JAN 2010

Abstract We use data from the first two dayside seasons of the Magnetospheric Multiscale (MMS) mission to study current systems associated with quasi-perpendicular bow shocks of generator type. We have analyzed 154 MMS bow shock crossings near the equatorial plane. We compute the current density during the crossings and conclude that the component perpendicular to the shock normal ($J_\perp$) is consistent with a pileup of the interplanetary magnetic field (IMF) inside the magnetosheath. For predominantly southward IMF, we observe a component J_n parallel (antiparallel) to the normal for GSM $Y > 0$ (< 0), and oppositely directed for northward IMF. This indicates current closure across the equatorial magnetosheath, and it is observed for IMF clock angles near 0° and 180°. To our knowledge, these are the first observational evidence for bow shock current closure across the magnetosheath. Since we observe no clear signatures of $|J_\perp|$ decreasing toward large $|Y|$ we suggest that the main region of current closure is further tailward, outside MMS probing region. For IMF clock angles near 90°, we find indications of the current system being tilted toward the north-south direction, obtaining a significant J_z component, and we suggest that the current closes off the equatorial plane at higher latitudes where the spacecraft are not probing. The observations are complicated for several reasons. For example, variations in the solar wind and the magnetospheric currents and loads affect the closure, and J_n is distributed over large regions, making it difficult to resolve inside the magnetosheath proper.

1. Introduction

At the bow shock, generator processes are active as the solar wind is decelerated and kinetic energy is converted into electromagnetic energy. A substantial part of the electromagnetic energy is converted back into particle energy in load processes when electrons and ions are reflected, accelerated, and heated, but a part is also transported toward the magnetosphere where it drives magnetospheric dynamics and energy conversion processes. Through theoretical arguments and numerical simulations it has been suggested that the Earth's bow shock is connected to the magnetospheric electric current systems via currents through the magnetosheath (Lopez et al., 2011; Siebert & Siscoe, 2002). For example, Siebert and Siscoe (2002) used simple circuit theory to argue that the magnetopause reconnection load must be connected to, and supplied by, a generator, and they identified the bow shock as the main generator region for the magnetopause loads, at least for the case of a quasi-perpendicular bow shock. Lopez et al. (2011) also used global magnetohydrodynamic (MHD) simulations to confirm that magnetopause loads are connected to the bow shock generator via electric currents.

The basic text-book picture is that the location of the magnetopause loads and generators will change as the interplanetary magnetic field (IMF) changes, and any current system connecting the bow shock to the magnetosphere must adapt. For example, load regions should dominate on the dayside magnetopause during southward IMF, while generators should exist tailward of the cusp in regions where the magnetic tangential force acts against the solar wind flow, causing the transfer of solar wind energy into magnetic energy density in the lobes (Siscoe & Cummings, 1969). During northward IMF, the location of loads and generators should be reversed, with generators existing equatorward and loads tailward of the cups. And for an arbitrary IMF, the location of the loads and generators can be shifted even more, and the bow shock-magnetospheric current system must adjust accordingly.

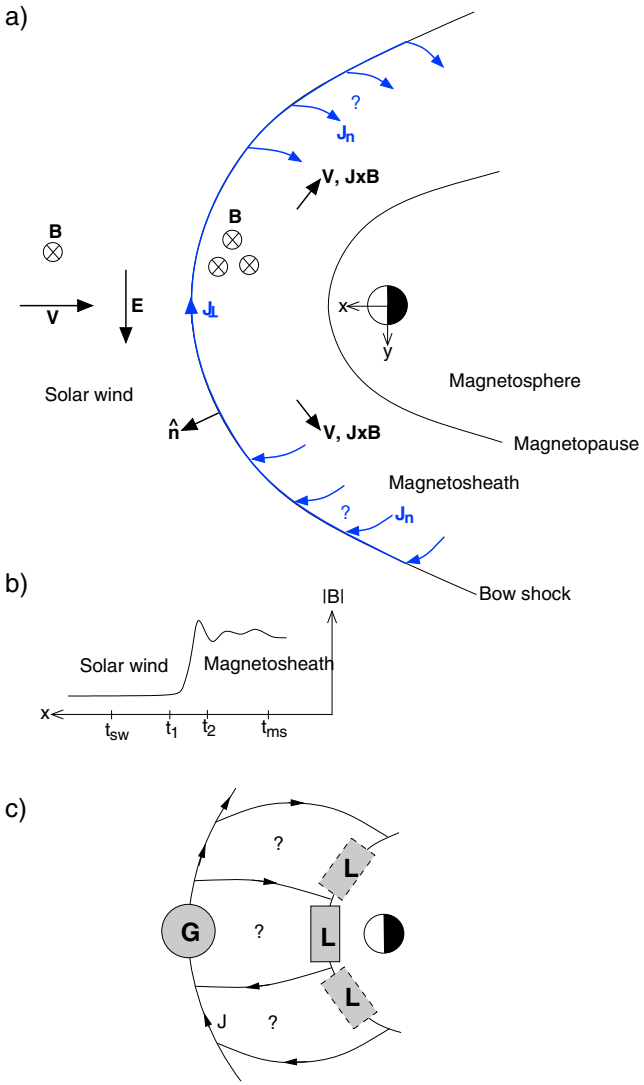

Figure 1. Schematic picture of (a,b) the magnetic field pileup during southward IMF and (a,c) the current system connecting the bow shock and the magnetosphere. In Figure 1b we indicate time values used in the event selection (see section 2): t_1 and t_2 are chosen to approximately enclose the main ramp signature in $|B|$, and t_{sw} and t_{ms} are chosen to represent the approximate undisturbed solar wind and magnetosheath (after any possible overshoot), respectively. See the text for a detailed explanation.

In Figure 1a we present a schematic picture of the bow shock and magnetosheath for the simple case of purely southward IMF B_z. The bow shock is classified as perpendicular since the IMF is oriented orthogonal to the bow shock normal, $\hat{\mathbf{n}}$. The magnetic field piles up behind the bow shock, and the pileup (Figure 1b) is sustained by an electric current component, $J_\perp = J_{\perp y}$ at the bow shock nose, perpendicular to the outward bow shock normal and running in the westward ($-y$) direction. The convective electric field, E, of the incoming solar wind is oriented in the eastward ($+y$) direction, opposite to this current, making the bow shock a generator (i.e., $\mathbf{E}\cdot\mathbf{J} < 0$). We have specifically chosen to present a perpendicular (or quasi-perpendicular in a more general case) bow shock of generator type in Figure 1. Such a bow shock is usually most easy to analyze observationally, since the signatures in the measured data are generally more clear (e.g., less reflected particles and wave activity disturbing the signatures) as compared to quasi-parallel shocks. Behind the bow shock, the plasma flow is diverted around the magnetosphere due to the $\mathbf{J}\times\mathbf{B}$ force. It is clear that the bow shock current in Figure 1a cannot close locally, or otherwise, it would not be capable of sustaining the magnetic field pileup in the magnetosheath. Instead, it must connect to the magnetospheric current systems, hereby allowing the bow shock generator to drive various magnetospheric load processes such as magnetopause reconnection (Lopez et al., 2011; Siebert & Siscoe, 2002). At least close to the bow shock, we therefore expect to find a J_n current component parallel or antiparallel to the bow shock normal. The blue arrows in Figure 1, hence, outlines parts of a clockwise current closure system, at least in the equatorial plane. The current then connects through the magnetosheath toward the magnetosphere, but it is possibly small and distributed over large regions, making it difficult to resolve with observed data. One important question is where the bow shock current closes (or diverges) toward the magnetosphere, and how this closure varies with, for example, changes in the solar wind and the IMF, as well as with changes in the geomagnetic activity and in the magnetospheric current systems, loads, and generators (Figure 1c).

It should be noted that even though Figure 1a corresponds to IMF $B_z < 0$ and $B_x = B_y = 0$, there are reasons to believe that the picture will be qualitatively similar for an oppositely directed IMF (i.e., $B_z > 0$) but with the direction of both E and J reversed, still making the bow shock a generator (Lopez et al., 2011). However, for an arbitrary IMF, it is likely that the bow shock in-plane $J_\perp$ is tilted away from the xy plane, obtaining a significant $J_{\perp z}$ component.

One can hence expect that the bow shock-magnetospheric current system will change significantly as the IMF changes, and as the location of the magnetopause loads and generators change in response to the IMF. Therefore, a detailed understanding of the magnetospheric energy conversion is also needed to understand the closure of the bow shock current. Laitinen et al. (2007) used global MHD simulations to study the location of magnetopause loads and generators, and they showed that the efficiency of the energy conversion depends on the IMF direction. For predominantly southward IMF, they found that almost the entire subsolar region corresponds to a reconnection load, while generators were found at high latitudes. For northward IMF, magnetopause energy conversion was found to be more irregular. The understanding of magnetospheric energy conversion has increased substantially through observational investigations using multispacecraft data from the Cluster and Magnetospheric Multiscale (MMS) missions. Such data enable detailed investigations of, for example, the current density ($\mathbf{J}\approx\nabla\times\mathbf{B}/\mu_0$). Some of the first experimental investigations of magnetospheric energy conversion regions were conducted using Cluster data of $\mathbf{E}\cdot\mathbf{J}$ from the tail plasma sheet (Hamrin et al., 2011, 2006; Marghitu et al., 2006) and from the magnetopause (Rosenqvist et al., 2006; Rosenqvist, Opgenoorth, et al., 2008; Rosenqvist, Vaivads, et al., 2008). Anekallu et al. (2013) used Cluster data to statistically investigate the local energy conversion at Earth's magnetopause during both dayside and lobe reconnection, and as a function of IMF and

solar wind dynamic pressure. For dayside reconnection, they found indications of an energy conversion pattern similar to what is expected with loads dominating equatorward and generators tailward of the cusps. However, they also noted several deviations from the basic picture. For example, load and generator regions were observed to be considerably scattered over the magnetopause surface. They also observed that the energy conversion increases for high dynamic pressures and large IMF magnitudes.

Only a few attempts to map the currents between the bow shock and magnetosphere have been reported in the literature. Most of them have been based on global simulations. For example, both Siebert and Siscoe (2002) and Lopez et al. (2011) used global MHD simulations to investigate the current closure, and they observed currents between the bow shock and the magnetosphere in the dayside magnetosheath, but at different latitudes. Siebert and Siscoe (2002) found a current closure through the magnetosheath in the equatorial plane for southward IMF, and at higher latitudes for northward IMF. Lopez et al. (2011), on the other hand, mainly focused on the case of southward IMF, for which they observed a current closure at higher latitudes. Similar to the observations of Anekallu et al. (2013), Lopez et al. (2011) also found that the high-latitude generators behind the cusps practically vanish for strong southward IMF and low Alfvén Mach numbers (or magnetically dominated plasmas, i.e., plasmas with the ratio between the plasma and magnetic pressures small, $\beta < 1$). This indicates a deviation from the simplest text-book picture of loads equatorward (tailward) and generators tailward (equatorward) for southward (northward) IMF, and they found that the bow shock is the only significant generator in the system for strong southward IMF. It has also been suggested that the bow shock can connect to other magnetospheric current systems such as the region 1 field-aligned current (FAC) system (Fedder et al., 1997; Guo et al., 2008; Siscoe & Siebert, 2006). For example, Guo et al. (2008) used global MHD simulations to show that the bow shock can contribute significantly to the region 1 FAC for strong southward IMF, high solar wind speeds, and large ionospheric Pedersen conductances. Global MHD simulations were also used by Tang et al. (2009) who showed that the bow shock can connect to the magnetospheric cross-tail current at high latitudes and that the contributions to this current system increase with increasing southward IMF and with increasing Pedersen conductance.

However, in the literature, there is a clear lack of observational studies of how the bow shock currents connect to the magnetosphere. Some hints for possible bow shock contributions to the magnetospheric current systems were obtained by Tang et al. (2012) in a small statistical study using Cluster data of 25 quasi-perpendicular bow shocks crossings and nine crossings of the high-latitude magnetopause. They observed that the bow shock current increases, but the high-latitude magnetopause surface current decreases, for stronger southward IMF. Assuming that general current systems in the magnetosphere typically get stronger for strong southward IMF, they argued that bow shock could indeed contribute to the magnetospheric current systems.

In this article we will extend the understanding of the bow shock current closure through a statistical investigation using MMS observations of quasi-perpendicular bow shocks of generator type observed close to the equatorial plane. We will show evidence of a closure of the bow shock current system toward the magnetosphere in a clockwise sense for predominantly southward IMF, and in an anticlockwise sense for predominantly northward IMF. For an IMF with a substantial east-west component, we will show indications of a tilt of the current system toward the north-south direction, and with a possible closure at higher latitudes. To our knowledge, this is the first piece of observational evidence for the closure of the bow shock current across the magnetosheath. The data and the event selection are presented in section 2. In section 3 we present two example events with different upstream IMF conditions as well as the results from the statistical study. Our results are summarized and discussed in section 4.

2. Data and Event Selection

In this investigation we use data from the MMS mission to study bow shock generator current systems. The four MMS spacecraft were launched in 2015 into a low-inclination orbit with perigee 1.2 R_E and apogee 12 R_E during the first mission phase. The orbit enables investigations of bow shock crossings approximately in the equatorial plane and earthward of ~12 R_E. We study bow shock passages from two MMS dayside seasons, October 2015 to February 2016 and October 2016 to February 2017, and we use fast survey mode magnetic field (16 s^{-1}) and electric field (32 s^{-1}) data from the FIELDS investigation, and ion moments from the Fast Plasma Investigation (4.5 s per sample) (Burch et al., 2015; Ergun et al., 2016; Lindqvist et al., 2016;

Pollock et al., 2016; Russell et al., 2014; Torbert et al., 2014). Throughout the article we use the GSM (Geocentric Solar Magnetospheric) coordinate system.

For the event selection we first choose time intervals with possible bow shock crossings by manually searching for transitions between isothermal and shocked solar wind plasmas in ion energy-time overview spectrograms. These intervals are then studied in more detail using fast survey mode data of the magnetic field (**B**), the electric field (**E**), and the ion energy-time spectrograms. By visual inspection, we search for clear bow shock crossings in the magnetic field data, and the start and stop times, t_1 and t_2, of the events are chosen manually so that the main shock ramp signature in $|B|$ is captured. To be able to study the changes over the bow shock, we also select t_{sw} and t_{ms} corresponding to time values in the approximate undisturbed solar wind and in the magnetosheath (after any possible overshoot), respectively. See also Figure 1b where these time values are schematically indicated. To keep only the simplest events, we also require that the magnetic field components, B_x, B_y, and B_z, on average must have the same sign at t_{sw} and at t_{ms} (average computed for $\Delta t = t_1 - t_2$ long time intervals). Such events are likely to be more stable since the upstream and downstream conditions are qualitatively quite similar. Moreover, we exclude events where there are so rapid back-and-forth oscillations of the bow shock over the spacecraft so that clear values of t_{sw} and t_{ms} cannot be chosen. We therefore require that the time between bow shock crossings should be longer that $\sim 2\Delta t$.

A high degree of reflected as well as heated particles (Burgess et al., 2012; Eastwood et al., 2005) is likely to affect the energy conversion properties of the bow shock, since particle energization corresponds to load processes. Hence, since we focus on studying bow shocks of generator type (i.e., the simplest type), we only keep events with a limited amount of upstream reflected ions in the spectrograms, and events for which the energy conversion over the shock is negative, that is, $\int_{t_1}^{t_2} \mathbf{E} \cdot \mathbf{J} dt < 0$, where the time integral is approximated with a cumulative sum over the event multiplied by the data sampling time.

The curlometer method is used for computing the current density (Dunlop & Eastwood, 2008). This is a multispacecraft method, and **J** can be considered to correspond to the current density averaged over the MMS tetrahedron which has a scale length of ~11 km during our events. Hence, it should be multiplied with the average electric field to obtain $\mathbf{E} \cdot \mathbf{J}$. However, the electric field measurements from the four spacecraft are very similar since the spacecraft are closely spaced, and we can therefore approximate **E** with the electric field obtained with only one of the spacecraft. In our case we have chosen spacecraft MMS1. The curlometer is based on the assumption that the magnetic field varies linearly between the spacecraft, and the estimate is often more accurate for spacecraft configurations which are rather close to equilateral, typically with both the elongation (E) and the planarity (L)$\lesssim 0.6$ (Dunlop & Eastwood, 2008; Paschmann & Schwartz, 2000). To estimate the error in the current calculation, one often computes the quantity $|\nabla \cdot \mathbf{B}|/|\nabla \times \mathbf{B}|$ (using the same data as for the current calculation), even though such an estimate cannot give a one-to-one correspondence to the true error. In theory, $|\nabla \cdot \mathbf{B}|/|\nabla \times \mathbf{B}| \equiv 0$, and the estimated ratio should be very close 0, but it can vary quite substantially from this. An often used upper limit is ~50%. For this investigation we only keep events where on average $E, L \lesssim 0.6$ over the events. For a majority (75%) of them we have estimated $|\nabla \cdot \mathbf{B}|/|\nabla \times \mathbf{B}|$ to be $\lesssim$25%. In total we end up with 154 generator bow shock events for our investigation.

The electric field is not invariant under Galilean velocity transformations, but the current density is. It is therefore important to use a correct frame of reference when analyzing energy conversion processes using the power density. Typically, one should use a frame in which a major part of the energy dissipation takes place (see Hamrin et al., 2012, for a more detailed discussion of reference frames and the power density). For this investigation, there are two possible frames of reference: (1) A frame which is stationary with respect to the Earth and (2) a frame which is stationary with respect to the bow shock. (1): It is well known that several important energy dissipation processes in geospace can be studied in frames which are approximately stationary with respect to the Earth (or in frames moving quite slowly relative to the Earth, at least when compared to other typical plasma flow velocities), since the inner magnetosphere and the ionosphere are two major energy sinks for the magnetospheric energy budget. For example, the amount of energy dissipated in the ring current and as auroral Joule heating and charged particle precipitation in the ionosphere is comparable to the energy dissipated in the plasma sheet, for example, in the form of plasmoid ejection and ion heating (see, e.g., Ieda et al., 2001, and Slavin et al., 1993). (2): The bow shock is also associated with important energy transfer processes. At the bow shock, the incoming solar wind is slowed down, kinetic energy of the bulk flow is converted into thermal energy, and parts of the solar wind energy are transported away as Poynting flux toward the magnetosphere where it drives various processes (e.g., Russell, 1985). The bow shock is also a region of

Table 1
Properties of Our 154 Events Described as 25%, 50%, and 75% Percentiles

Properties	25%	50%	75%
Location			
Δt (s)	7	12	20
X GSM (R_E)	10.0	11.0	11.4
Y GSM (R_E)	−3.0	0.9	3.6
Z GSM (R_E)	−2.4	−1.4	−0.7
Bow shock configuration			
Normal GSM $\hat{n}_x$	0.97	0.98	0.99
Normal GSM $\hat{n}_y$	−0.14	0.05	0.18
Normal GSM $\hat{n}_z$	−0.04	−0.04	0.01
Shock angle (deg)	74	99	116
Solar wind			
Velocity $\lvert V_x \rvert$ (km/s)	372	412	516
Density (cm^{-3})	9	11	16
Dynamic pressure (nPa)	2.9	4.1	5.3
Alfvén Mach number	7.1	8.8	10.8
Plasma β	9	15	39
IMF, $\lvert \mathbf{B} \rvert$ (nT)	5.8	8.1	10.2
IMF B_z component (nT)	−4.8	−2.0	3.0
Clock angle, $\lvert \theta \rvert$ (deg)	66	107	137
Electric field, $\lvert \mathbf{E} \rvert$ (mV/m)	2.0	3.1	4.3
MMS tetrahedron and curlometer			
Elongation, E	0.09	0.15	0.23
Planarity, P	0.24	0.28	0.33
$\lvert \nabla \cdot \mathbf{B} \rvert / \lvert \nabla \times \mathbf{B} \rvert$ (%)	14.1	17.5	24.6
Energy conversion			
$\int \mathbf{E} \cdot \mathbf{J} dt$ (μJ/m^3)	−21	−11	−6

intense particle acceleration, and the energetic ions and electrons in the upstream foreshock regions supply free energy for wave growth (Burgess et al., 2012).

For our statistical investigation we evaluate the power density in a frame which is at rest with respect to the Earth, since we believe that this best describes the energy conversion properties of the entire solar wind-magnetosphere-ionosphere system. However, it is important to understand how much the electric field, and hence $\mathbf{E} \cdot \mathbf{J}$, would change if we instead used a frame moving with the bow shock. It can be difficult to obtain very accurate values of the bow shock motion, but typical velocities of the terrestrial bow shock are found to be of the order of 0–120 km/s (Maksimovic et al., 2003). For a typical value of the IMF of ∼10 nT, the correction to the electric field due to transformations between a frame at rest with respect to the Earth and a frame moving with the bow shock is hence $|\Delta E| \lesssim 1$ mV/m. This is in general smaller than the median of the observed electric field during our events which is approximately 3.1 mV/m (see Table 1).

3. Observations

In total we have selected 154 clear bow shock events of generator type for this study, 108 are observed during the first (2015–2016) and 46 during the second dayside season (2016–2017). In Table 1 we give an overview of the distribution of some properties of the events. The properties are expressed as 25%, 50%, and 75% percentiles. All quantities concerning the location of the events and the solar wind are based only on data from MMS spacecraft 1 (and data from the OMNI web for the shock normal properties), while data from all four MMS spacecraft are used for computing the other quantities.

From Table 1 we see that the median duration of the events is 12 s and that the events are distributed slightly duskward of the noon-midnight meridian, with a median value of $Y \approx 0.9\ R_E$. This shift toward $Y > 0$ is reasonable since we expect our events to be quasi-perpendicular, and such events should be more common toward dusk due to the overall Parker spiral behavior of the solar wind since only events with little or negligible ion reflection have been selected, it is likely that they are of more quasi-perpendicular character (Bale et al., 2005; Burgess et al., 2005). Fluctuations in the IMF can of course cause deviations from this simple picture, but a little more than half of our events (∼56%) are observed for GSM $Y > 0$. Moreover, all events are observed within $-6.8\ R_E < Y < 8.6\ R_E$, and 13 events are observed for $Y > 6\ R_E$ but only 6 for $Y < -6\ R_E$ (not shown).

For nominal upstream solar wind conditions, the subsolar bow shock is typically located at $\sim 14\ R_E$ (see, e.g., Dmitriev et al., 2003; Merka et al., 2003), but during disturbed conditions, the magnetosphere is compressed and the bow shock can be significantly displaced toward the Earth. Since the apogeum of the MMS orbit ($12\ R_E$) is Earthward of the nominal bow shock position, the events included in our investigation will therefore typically be associated with disturbed solar wind conditions. From Table 1, we see that our events are observed at a median value of $X \sim 11\ R_E$. However, it should be noted that this value is reduced also due to the fact that it is obtained using all events distributed over the available Y range and that the bow shock is located at smaller X values toward the flanks. No detailed investigation of the location of the individual bow shock crossings has been conducted since this is outside the scope of the present investigation, but a quick survey (not shown) indicates that a significant fraction of the events indeed have the upstream ion velocity and/or density increased, possibly causing the bow shock being displaced toward the Earth. In Table 1 we present percentile values of various solar wind parameters (within a time interval $\Delta t = t_2 - t_1$ centered around t_{sw}—see section 2): the solar wind velocity, density, dynamic pressure, Alfvén Mach number, plasma β, and IMF magnitude. We see that some parameters are close to nominal (e.g., the solar wind velocity), even though individual events can show quite substantial elevated values, while others (e.g., the dynamic pressure) are higher than normal values.

For all our events, we have computed the bow shock normal with the Farris and Russell (1994) model using OMNI solar wind data propagated to the nominal bow shock nose point (https://omniweb.gsfc.nasa.gov/). From Table 1 we see that the shock normal for a clear majority of our event are closely aligned with the GSM x direction, with a median normal of $N = [0.98, 0.05, -0.04]$. This orientation of the normal is reasonable since our events are observed relatively close to the subsolar point (see the discussion above). We have also computed the approximate angle between the bow shock normal and the upstream IMF observed with MMS at t_{sw}, and we find that our events typically correspond to quasi-perpendicular bow shocks since the median shock angle is 99° which is close to perpendicular.

The IMF clock angle is computed as the angle between GSM north and the median IMF direction within a time interval Δt centered around t_{sw}. Our events are observed within a large range of clock angles, $2° < |\theta| < 180°$ (not shown), but a majority of them are observed for southward IMF conditions with a median of ~107° (see Table 1), and with 25% and 75% percentiles of 66° and 137° , respectively.

The last line of Table 1 contains the value of the power density integrated over the main shock ramp of the events, $\int_{t_1}^{t_2} \mathbf{E} \cdot \mathbf{J} dt$. We can see that the events have been selected to be bow shock crossings of generator character (see section 2) since $\int_{t_1}^{t_2} \mathbf{E} \cdot \mathbf{J} dt < 0$ for all events. The median value is −11 μJ/m^3.

3.1. Example Event 1: IMF B_z Southward and Large Clock Angle, $|\theta| \approx 162°$

In Figure 2 we show overview data for a bow shock crossing for which the upstream IMF is southward with a large clock angle. The IMF conditions for this event are hence favorable for subsolar magnetopause reconnection, and they are similar to what is presented in the schematic sketch in Figure 1. The event was observed on 7 October 2015, around 13:46:40 UTC, and it is highlighted in yellow. Another bow shock crossing from the same day at ~11:44:45 UTC has previously been discussed by Johlander et al. (2016) who showed that ripples existed on the shock surface during that event.

Figures 2a–2d show the energy-time spectrogram for ions, the ion density, and the GSM components of the ion velocity and the magnetic field, respectively. We see that the MMS spacecraft come from the solar wind to the left and cross through the bow shock into the magnetosheath to the right, and the yellow region approximately contains the ramp-like features of the shock in the magnetic field (cf. Figure 1b). From the upstream solar wind MMS data of the magnetic field we have estimated the clock angle $|\theta| \approx 162°$. The event is observed on the duskside flank approximately at $XYZ = [7.2, 8.0, 5.2]\ R_E$. The upstream solar wind velocity is close to nominal values, $|Vx| \approx 400$ km/s, while the ion density is elevated, $N \approx 24$ cm^{-3}. The value of the upstream dynamic pressure is hence also clearly elevated, $P_{dyn} \approx 12$ nPa, while the Alfvén Mach number and the plasma β are close to typical values, ~7 and ~10 (not shown).

Estimating $|\nabla \cdot \mathbf{B}|/|\nabla \times \mathbf{B}|$, we find that it is ≈29% for this event (i.e., smaller than the often used threshold of 50%), $E \approx 0.03$, and $P \approx 0.6$. These values are hence small enough for multispacecraft data to be useful for estimating spatial gradients, and for using the curlometer to compute the current density (Dunlop & Eastwood, 2008). We can therefore estimate both $\mathbf{E} \cdot \mathbf{J}$ and $\nabla \cdot \mathbf{S}$, where $\mathbf{S} = \mathbf{E} \times \mathbf{B}/\mu_0$ is the Poynting flux. The result is shown in Figure 2e. Both the red and black curves exhibit significant fluctuations, but a detailed inspection shows that in general $\mathbf{E} \cdot \mathbf{J} < 0$ and $\nabla \cdot \mathbf{S} \approx -\mathbf{E} \cdot \mathbf{J}$. Hence, according to Poynting's theorem, $\partial B^2/\partial t (2\mu_0)^{-1} = -\nabla \cdot \mathbf{S} - \mathbf{E} \cdot \mathbf{J} \approx 0$. We conclude that this is a bow shock of generator type, that changes in the local magnetic field energy density are negligible, and that most of the energy should be transported away as Poynting flux.

The energy conversion properties of the event are easier to analyze using the time integral of the power density along the spacecraft path. In Figure 2f we show the resulting integral of the total power density $\mathbf{E} \cdot \mathbf{J}$ (thick black curve) and of the GSM $E_x J_x$, $E_y J_y$, and $E_z J_z$ components (thin black, blue, and red lines). The generator character of the event can be confirmed since $\int \mathbf{E} \cdot \mathbf{J} dt \approx -12$ nJ/m$^3 < 0$ over the event. We also see that the main generator signature comes from the east-west current system since $\int E_y J_y dt$ show a significant drop during the highlighted region, while $\int E_x J_x dt$ and $\int E_z J_z dt$ are weakly positive. This is consistent with the simple picture in Figure 1a, where a southward IMF is associated with a westward generator current on the bow shock.

Using a simple timing method on the magnetic field data from the four MMS spacecraft, we can estimate the direction and the speed the bow shock, and we find that the speed is small, $|V_{bs}| \approx 10$ km/s. Hence, if we would transform the observed electric field to a frame in rest with respect to the bow shock, the corrections to the electric field will be of the order of $|\Delta E| \approx |V_{bs} B|$, which is ~0.15 mV/m in the solar wind (using $B_{sw} \approx 15$ nT) and ~0.5 mV/m inside the magnetosheath (using $B_{ms} \approx 40$ nT). $|\Delta E|$ is hence negligible as compared to the

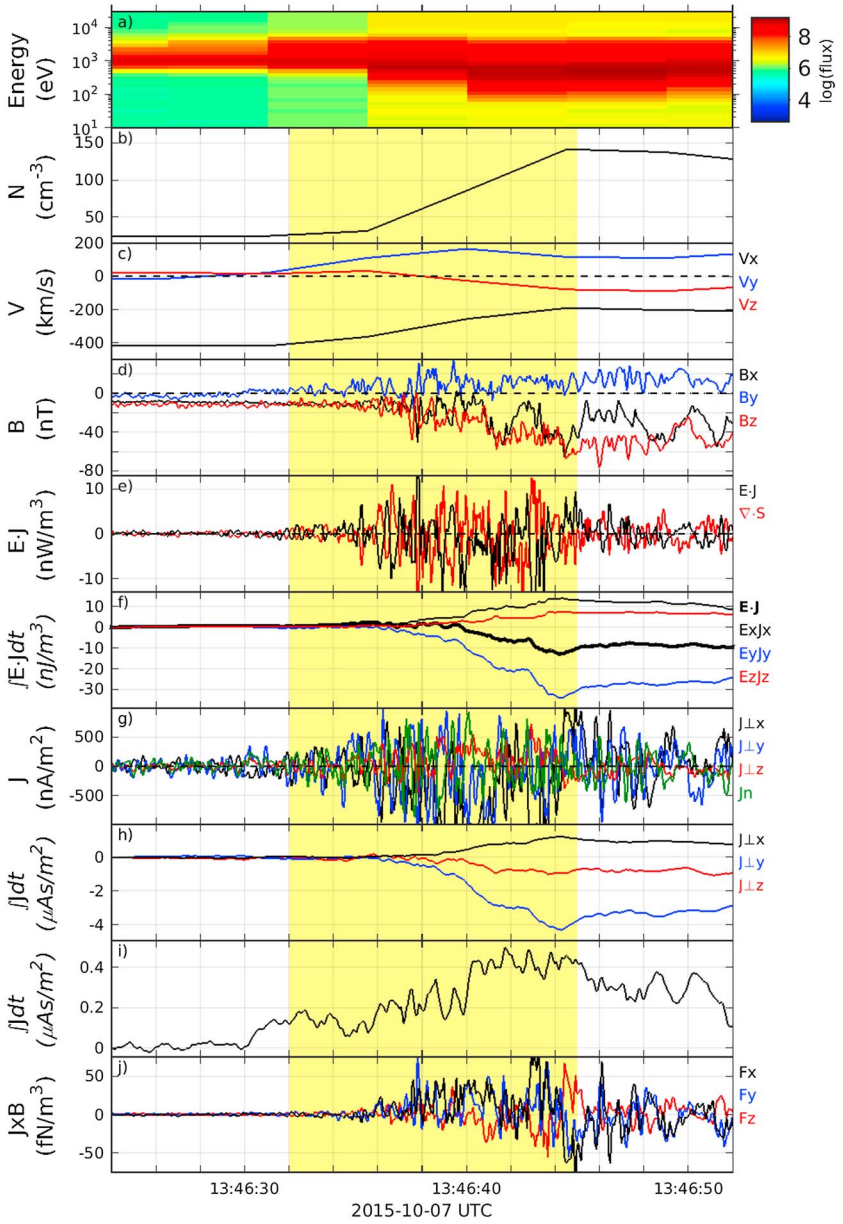

Figure 2. Example of an event for a southward upstream IMF (large solar wind clock angle). (a) Ion energy-time spectrogram. (b) Ion density. (c, d) GSM components of the ion bulk velocity and the magnetic field. (e) Power density and the divergence of the Poynting flux. (f) Time integral of the total power density (thick black line) and the separate GSM components (black, blue, and red). (g) GSM components of the current density perpendicular to the outward bow shock normal (black, blue, and red) and the current density along the normal (green). (h, i) Time integral along the spacecraft path of the current density from the previous panel. (j) GSM components of the $\mathbf{J} \times \mathbf{B}$ force. The event is indicated in yellow, and it captures the main part of the shock ramp in the magnetic field. The data in Figures 2a–2d are obtained from spacecraft MMS 1, and the other data from all four spacecraft.

electric field observed in the solar wind and the magnetosheath, ~5 mV/m and ~7 mV/m (not shown), and we conclude that it is fully appropriate to estimate the power density in the frame of the Earth.

To study the orientation of the bow shock current system in more detail, we analyze its components in a system defined by the bow shock normal. The normal direction has been determined through minimum variance analysis (MVA) using magnetic field data from MMS 1, and through timing between spacecraft using data from all four satellites, respectively. Both methods result in approximately the same outward normal, $\hat{\mathbf{n}} \approx [0.93, 0.31, -0.21]$. We have also estimated $\hat{\mathbf{n}}$ with the Farris and Russell (1994) bow shock model using upstream solar wind data from the OMNI database, and we find that the model gives a fully consistent result.

In Figure 2g we present the current density in a plane perpendicular to $\hat{\mathbf{n}}$ ($J_\perp$) and along $\hat{\mathbf{n}}$ (J_n), respectively. It is important to note that we have chosen to express $J_\perp$ in Figure 2g with its three GSM *xyz* components (black, blue, and red curves). This we have done to be consistent with what is used in our statistical investigation (section 3.3) where we approximate J_n with J_x, and $J_\perp$, with J_y. This is a valid approximation since the bow shock normal of the individual events are closely aligned with the GSM *x* direction (see Table 1). From Figure 2g we see that the components of the current exhibit substantial fluctuations, but a detailed zoom onto the data (not shown) reveals a general trend of $J_{\perp y}$ and J_n on the average being negative and positive, respectively. To better capture the general trend of the current components, we compute the time integral along the spacecraft path (i.e., accumulating the current density in a sum from 13:46:24 UTC and onward in time and multiplying with the sampling time). The result is presented in Figures 2h and 2i. By dividing the total change in the integrated currents over the event (yellow region in Figure 2) by the time duration of the event, we can compute the mean of the bow shock current density components. From Figure 2h see that there is a clear westward component of the bow current since $\int J_{\perp y} dt$ shows a clear decrease over the event, and the mean value of $J_{\perp y}$ is approximately $-3.9\,\mu A s/m^2$ divided by the duration of the event (13 s), that is, approximately $-300\,nA/m^2$ which is consistent with a detailed zoom in Figure 2g. The other two components, $J_{\perp x}$ and $J_{\perp z}$, are small but weakly positive. The result is fully consistent with the sketch in Figure 1a, where a westward current is needed to sustain the pileup of a southward magnetic field in the magnetosheath.

After the event, the cumulative sums of the current density components appear to level out at quite stable values, indicating a negligible current density. However, the curlometer method is not entirely reliable for current density calculations outside the event: In the solar wind $|\nabla\cdot\mathbf{B}|/|\nabla\times\mathbf{B}|$ is estimated to be elevated (~43%, often reaching values >100%), and in the magnetosheath the magnetic field is highly fluctuating, possibly showing both spatial and temporal variations. Moreover, it is likely that any global currents passing through the magnetosheath and connecting to the bow shock are distributed over large regions. They should hence be small and difficult to resolve. Indeed, a manual survey of all events included in our database indicate that the noise level of the curlometer current in the magnetosheath proper may well be too large to resolve any true currents. Overall, this implies that no clear conclusions can be drawn about the current density outside our events.

From Figure 2i we see that the current density along the outward normal is positive during the event since $\int J_n dt$ shows an increase, and the mean value over the event is $\sim 0.33/13\,\mu A/m^2 \approx 25 nA/m^2$, which is consistent with Figure 2g. Due to the direction of the bow shock normal, $\hat{\mathbf{n}} \approx [0.93, 0.31, -0.21]$, this means that there is a current component approximately in the positive GSM *x* direction. Since the event is observed on the duskward side on the bow shock, the normal component of the current density is oriented in the same sense as illustrated in Figure 1a. This indicates that the current system for this event may well close across the magnetosheath toward the bow shock as illustrated in Figure 1a.

The normal current component, $|J_n|$, is approximately 1 order of magnitude less than the perpendicular component, $|J_{\perp y}|$. This is also consistent with Figure 1a where the divergence of the current density (from the normal to the perpendicular direction) is distributed over an extended spatial region along the bow shock, while $|J_\perp|$ is concentrated to the thin shock. However, note that we cannot make any clear conclusions about the current component further inside the magnetosheath as discussed above.

In the last panel of Figure 2 we show the GSM components of force $\mathbf{F} = \mathbf{J} \times \mathbf{B}$. All force components show substantial fluctuations over the event, but on the average both F_x and F_y are positive, while F_z oscillates more around zero. A positive value of F_x is consistent with the deceleration of the incoming solar wind at the bow shock, while the positive value of F_y is consistent with the deviation of the shocked solar wind around the magnetosphere, that is, a force in the eastward direction on the duskside.

3.2. Example Event 2: IMF B_z Northward and Intermediate Clock Angle, $|\theta| \approx 49°$

In Figure 3 we show an example where the IMF has a significant northward component and a nonnegligible $B_y > 0$ (clock angle $|\theta| \approx 49°$). It is observed on 21 October 2015, around 09:04:15 UTC at the duskward side on the bow shock, $XYZ \approx [10, 5, -3.6]\,R_E$. The MMS spacecraft cross the bow shock from the solar wind to the magnetosheath, and the upstream values of the density (~18 cm^{-3}) and the plasma β (~60, not shown) are higher than nominal, while the velocity $|V_x|$ (~350 km/s) and the Alfvén Mach number (~10, not shown) are more close to typical values. The normal direction has been computed with MVA, timing, and the Farris and Russell (1994) bow shock model, and we find that $\hat{\mathbf{n}} \approx [0.97, 0.20, -0.15]$.

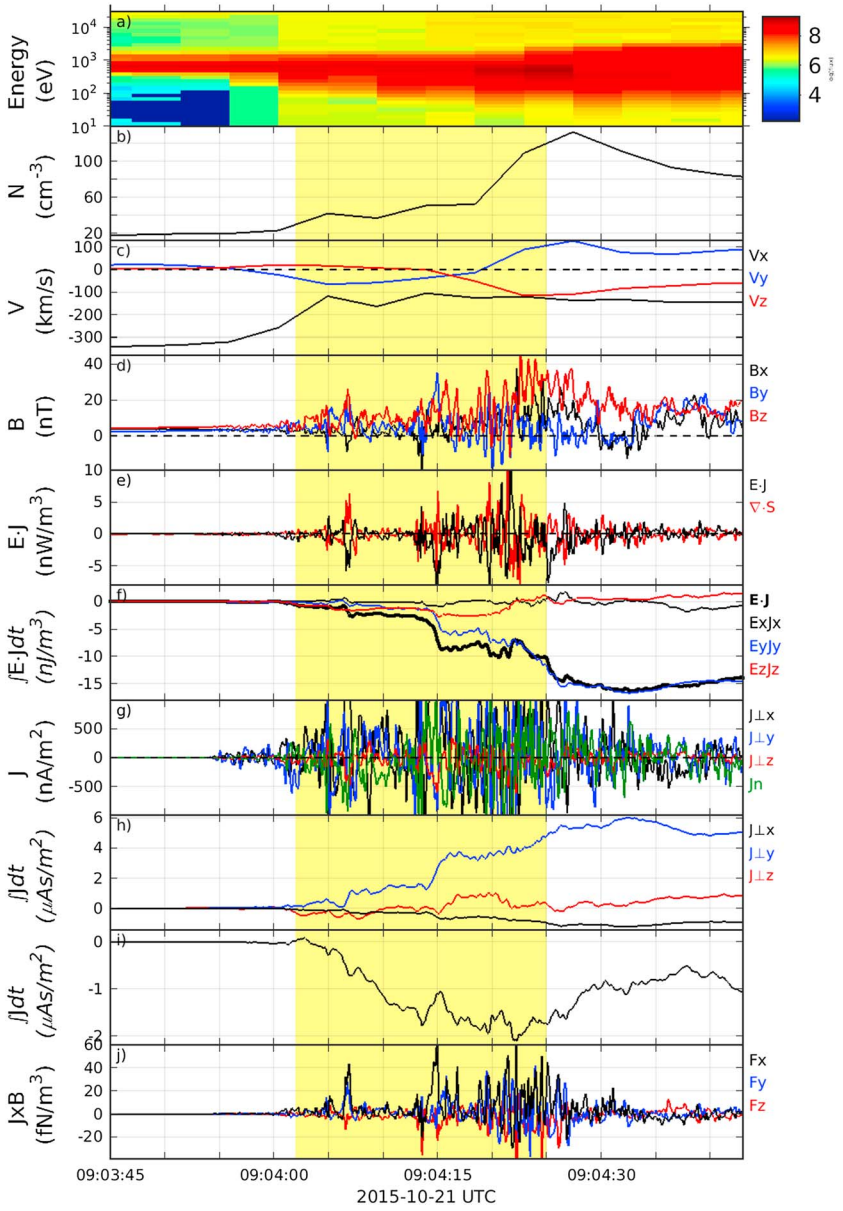

Figure 3. Same as Figure 2 but for northward IMF (small clock angle).

From Figures 3e and 3f we see that also this event has $\nabla \cdot \mathbf{S} \approx -\mathbf{E} \cdot \mathbf{J}$ and $\int \mathbf{E} \cdot \mathbf{J} dt < 0$, with the main contribution to the generator properties coming from $E_y J_y$. Computing the speed of the bow shock using timing between the spacecraft, we find that $|V_{bs}| \approx 9$ km/s, resulting in $|\Delta E| \approx 0.05$ mV/m and 0.2 mV/m in the solar wind and magnetosheath, respectively, if the electric field should be transferred to a frame at rest with respect to the bow shock. This is again negligible as compared to observed electric fields, ~2 mV/m and ~3 mV/m in the solar wind and magnetosheath (not shown), and it is hence fully appropriate to estimate the power density in a frame at rest with respect to the Earth.

As discussed in section 1, it is likely that the current system at the bow shock is qualitatively similar for southward and northward IMF B_z (Lopez et al., 2011) but that it can be tilted away from the *xy* plane if there is a significant B_y component. From Figure 3h, we see that there is indeed an eastward current in the plane of the bow shock (mean value $\sim 5/23\,\mu A/m^2 \approx 220\,nA/m^2$), consistent with a pileup of an IMF with a northward component. However, for this specific case there are no clear indications of a tilt of the bow shock current system since $J_{\perp z}$ is small (similar to the first example event in Figure 2).

From Figure 3i we see that the current component in the normal direction is negative, (mean value $\sim -1.8/23\,\mu A/m^2 \approx -78\,nA/m^2$), for this event located on the duskward bow shock. This indicates a qualitatively similar current pattern as in Figure 1a but with the direction of B_z, $J_{\perp y}$, and J_n consistently reversed. Similar to the example in Figure 2, the event in Figure 3 has $|\int J_n dt| < |\int J_{\perp y} dt|$, which is consistent with the normal current being distributed over large areas. However, the ratio between the normal and perpendicular currents (as estimated from the highlighted yellow regions in Figures 2h, 2i, 3h, and 3i) is larger than for the previous event (~0.4 instead of ~0.1). This can be caused by, for example, variations in the upstream solar wind and IMF conditions, tilts of the electric current system from the *xy* plane (making the spacecraft probing a region with stronger normal currents for example event 2), and/or variations in the noise level of the estimated current. However, it is outside the scope of the present study to investigate this further, but it can be noted that inside event 2, we have estimated $|\nabla \cdot \mathbf{B}|/|\nabla \times \mathbf{B}|$ to be $\approx$ 20% (i.e., smaller than for example event 1, and significantly smaller than the threshold of 50%), $E \approx 0.06$, and $P \approx 0.4$, and the curlometer should be expected to work properly. However, similar to the first example event, we consider the curlometer less reliable outside the highlighted interval, so we cannot draw any clear conclusions about the current density here. Considering the $\mathbf{J} \times \mathbf{B}$ force in Figure 3j, it shows a consistent behavior with $F_x > 0$ decelerating the incoming solar wind and $F_y > 0$ deviating it around the duskward side of the magnetosphere.

3.3. Statistical Investigation

In Figure 4 we present the result from a superposed epoch study on a subset of the 154 events included in our database. The thick black line shows the median, and the thin lines indicate the 25% and 75% percentiles, respectively. The gray lines in the background show the corresponding data from all events, and the thin black lines correspond to the 25% and 75% percentiles, respectively. Events with a small clock angle $|\theta| \leq 50°$ (31 events) are presented to the left, and events with a large angle $|\theta| \geq 130°$ (47 events) are presented to the right. Consequently, B_z is predominantly northward in the left column and predominantly southward in the right one (see Figures 4a and 4b), while B_y can be either positive, negative, or very small. The time line for each event, $t_1 - 3\Delta t < t < t_2 + 3\Delta t$, has been normalized to one. Therefore, the main event (i.e., the main part of the shock ramp, see Figure 1 and section 2) is located within $0.43 \lesssim T \lesssim 0.57$ in Figure 4. The time line has also been adjusted so that upstream solar wind data are to the left and downstream magnetosheath data to the right.

Since our events are observed for quite small $|Y|$ values, the outward bow shock normal has in general a large GSM *x* component (see also Table 1), and we can therefore approximate the normal current J_n with the GSM J_x component. Similarly, we approximate the in-plane current $J_\perp$ with J_y. From Figures 4c and 4d we see that J_y in general is oriented eastward (westward) for a northward (southward) IMF. This is consistent with the magnetic field pileup in the magnetosheath and the simple picture in Figure 1a. Hence, we can conclude that the curlometer indeed gives accurate enough current density estimates over the events. Note also that magnitude of J_y is slightly larger in Figure 4c than in Figure 4d. This is consistent with the results of Samsonov (2006) who used MHD simulations to show that the bow shock current is larger for northward IMF than for other IMF orientations.

The J_x component has in Figures 4e and 4f been multiplied with the sign of the *Y* location of the events to keep track of the expected symmetry of the current system around $Y \sim 0$ (see the example in Figure 1a where the normal current is outward for $Y > 0$ and inward for $Y < 0$). From Figures 4e and 4f we see that $J_x Y/|Y|$ is small but weakly negative for small clock angles ($|\theta \leq 50°|$, Figure 4e) and weakly positive for large angles ($|\theta \geq 130°|$, Figure 4f). This is fully consistent with a divergence of the current needed for closure toward the magnetosphere, that is, with $\mathbf{J}_\perp$ connecting to an outward $\mathbf{J}_n$ on the duskside and an inward $\mathbf{J}_n$ on the dawnside for a southward IMF (as in Figure 1a) and directions of all the currents reversed for a northward IMF. We also see that $|J_n| \ll |J_\perp|$. This is reasonable since we expect $\mathbf{J}_n$ to be distributed over large regions in space. It is also possible that the main region of current closure is located, for example, at higher altitudes or further tailward, and that the MMS spacecraft only probe the outer parts of the current closure regions where the magnitude of the normal current would be smaller.

All events have been selected so that $\int_{t_1}^{t_2} \mathbf{E} \cdot \mathbf{J} dt < 0$. However, as seen from Figures 4g and 4h, the magnitude of the integrated power density can vary between the events, possibly due to variations in the upstream solar wind conditions, making the energy conversion capacity of the observed bow shocks vary. Moreover, from Figures 4i and 4j, we see that a significant part of the power density, on the average, comes from $E_y J_y$, and we conclude that the equatorial current system is important for the energy conversion capacity for

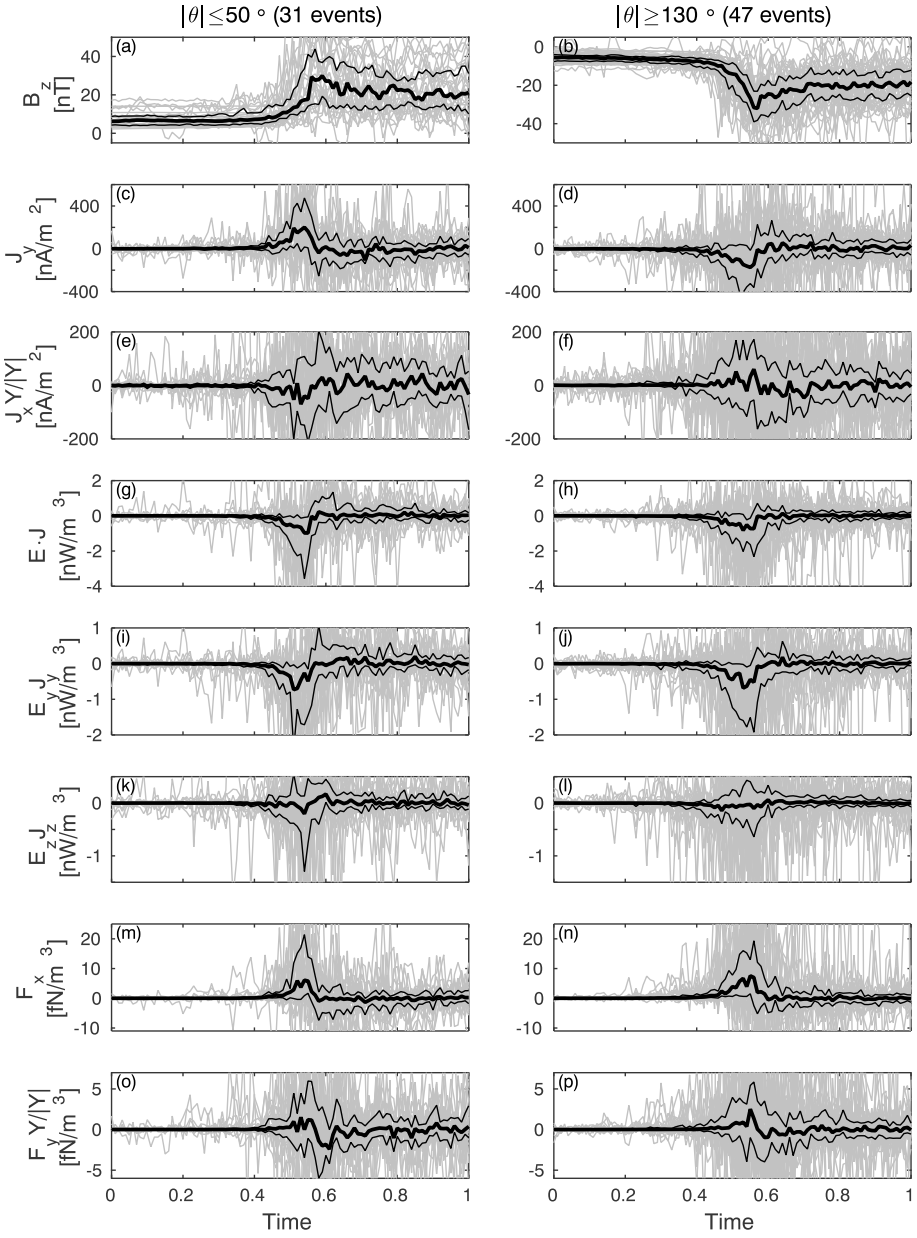

Figure 4. Superposed epoch study of events with IMF clock angle $|\theta| \leq 50°$ (left) and $|\theta| \geq 130°$ (right). (a–f) GSM z component of the magnetic filed and y and x components of the current density. The x component of the current has been multiplied with the sign of the Y position of the event to systematically make use of dawn-dusk symmetries at the bow shock. (g–l) Power density and the contribution from GSM E_yJ_y and E_zJ_z, respectively. (m, n) The component of the $\mathbf{J} \times \mathbf{B}$ force in the GSM x direction. (o, p) The y component of the force multiplied with the sign of the GSM Y position of the event. The gray lines indicate data from the events included and the thick black line, and the two thin lines show the median, and the 25% and 75% percentiles, respectively. The solar wind is to the left and the magnetosheath to the right, and the event (main shock ramp) is located in the time range $0.43 < t < 0.57$.

quasi-perpendicular bow shocks for which the IMF has either a small or a large clock angle. However, the contribution from E_zJ_z can either strengthen or weaken the total power density (Figures 4k and 4l).

As can be seen from Figures 4m and 4n, the x component of the $\mathbf{J} \times \mathbf{B}$ force, F_x, is in general positive. This is consistent with a deceleration of the incoming solar wind at the bow shock. To take care of a possible symmetry of F_y for events located on the duskside and dawnside bow shock, respectively, we have multiplied the F_y in Figures 4o and 4p with the sign of the Y position of the event, and we see that F_y is in general oriented

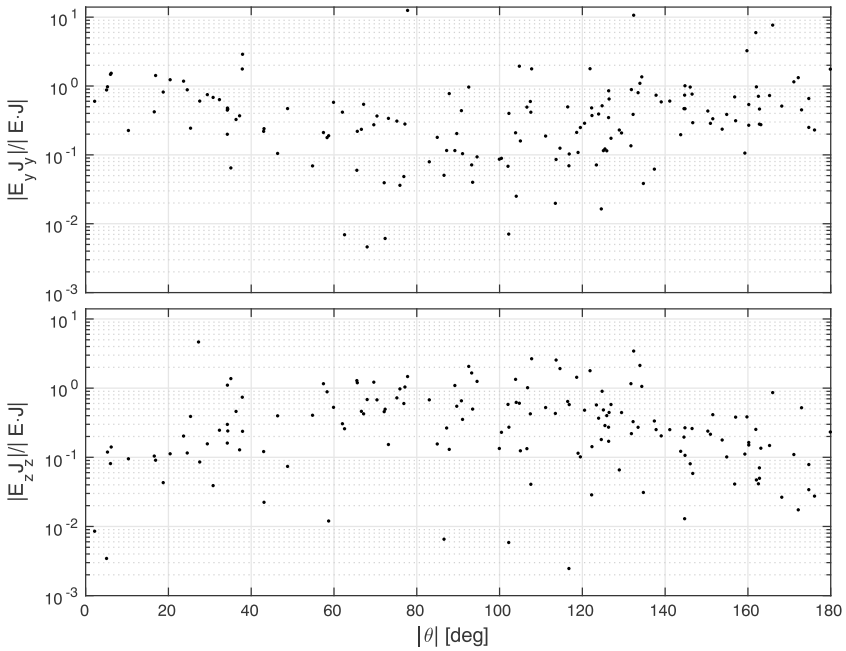

Figure 5. The contribution of $|E_y J_y|$ (top) and $|E_z J_z|$ (bottom) to the total power density as a function of clock angle $|\theta|$.

away from noon toward dusk (dawn) on the duskside (dawnside), consistent with a deviation of the plasma flow around Earth's magnetosphere.

As previously mentioned, it is likely that the current system is tilted away from the *xy* plane when IMF $|B_y|$ is large, that is, for clock angles close to 90°. In Figure 5 we show a scatterplot of the contribution of $|E_y J_y|$ (top) and $|E_z J_z|$ (bottom) to the total power density, and we see that the contribution to $|\mathbf{E} \cdot \mathbf{J}|$ from $|E_y J_y|$ becomes smaller, and the contribution from $|E_z J_z|$ becomes larger, for $|\theta|$ near 90°. This shows that the bow shock current system is likely to be tilted away from the *xy* plane, toward the north-south direction, when the upstream IMF has a significant $|B_y|$ component. Since the bow shock current system is expected to be connected through the magnetosheath to the magnetopause systems, one can speculate that this rotation coincides with a displacement of the magnetopause reconnection loads in response to the IMF variations.

Since our events in general are observed quite close to noon (see Table 1), we can approximate the normal current component with the component in the GSM *x* direction, that is, $J_n \approx J_x$. To study variations in this component, in Figure 6 we show scatterplots of J_x versus *Y* for five different clock angle ranges, with smallest angles at the top and largest at the bottom. The number of events presented in each subplot (*N*) is displayed in the upper right corner together with the slope (*a*) and the intercept (*b*) of a straight line fitted to the data. The values within the brackets indicate the 95% confidence intervals. We see that the slope is clearly negative for small clock angles ($0° \le |\theta| \le 50°$, Figure 6a), while it is clearly positive for large angles ($130° \le |\theta| \le 180°$, Figure 6e). This is true also within the error margins, and it shows a consistent current density pattern where the normal current is Earthward on the duskside and sunward on the dawnside for small angles, and opposite to this in the case of large angles (cf. Figure 1a). We therefore argue that the divergence of the current density near the bow shock is consistent with a current closure across the magnetosheath, at least for cases with a dominant IMF B_z north or south. However, as discussed before, the current density outside the events in the magnetosheath proper is probably too weak to be resolved with current methods and missions, and no clear conclusions can be drawn about the current system further inside the magnetosheath.

For angles close to perpendicular ($80° \le |\theta| \le 100°$) in Figure 6c, there are too few data points to obtain any reliable results, but for intermediate angles ($50° \le |\theta| \le 80°$ and $100° \le |\theta| \le 130°$) in Figures 6b and 6d, the statistics are better. However, we cannot see any clear signatures of an inward-outward current closure on the flanks (i.e., for large $|Y|$). One possible reason is that the bow shock current system is tilted away from the *xy* plane so that less of the current closure can be observed by the MMS spacecraft which are probing

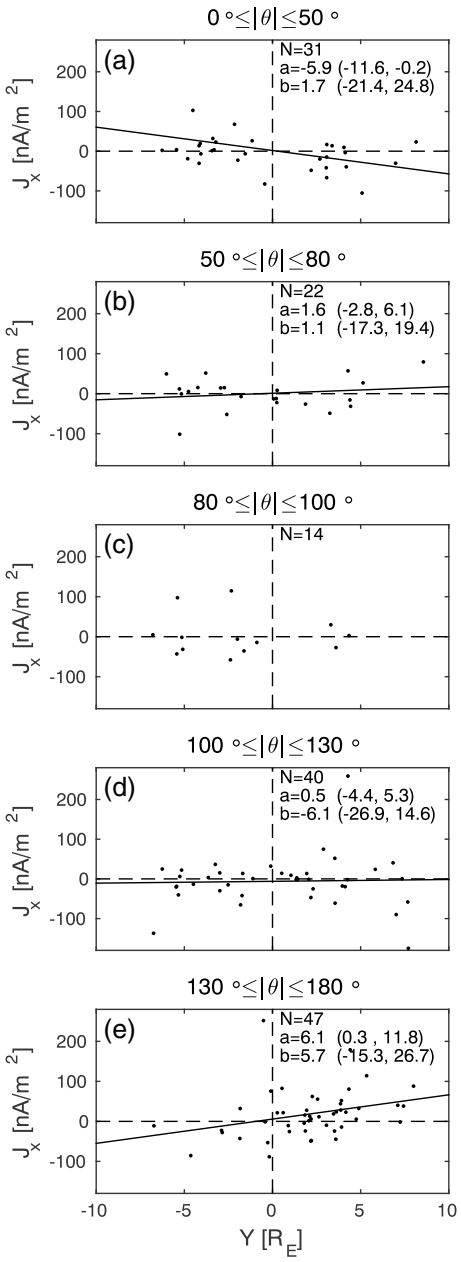

Figure 6. GSM J_x versus Y for five different clock angle ranges: (a) $0° \le |\theta| \le 50°$, (b) $50° \le |\theta| \le 80°$, (c) $80° \le |\theta| \le 100°$, (d) $100° \le |\theta| \le 130°$, and (e) $130° \le |\theta| \le 180°$.

approximately in the equatorial plane. This is consistent with the results from Figure 5 which clearly shows that the contribution to $\mathbf{E} \cdot \mathbf{J}$ from $E_z J_z$ increases and from $E_y J_y$ decreases for or IMF clock angles close to 80°.

As mentioned above and as indicated in Figure 1a, it is likely that J_n is distributed over large areas. Consequently, due to current continuity, the magnitude $|J_\perp|$ should decrease away from the subsolar point as more and more of $J_\perp$ is diverted toward the magnetosphere. One may therefore expect that the major region of current divergence toward the magnetosphere should manifest itself as an observable decrease of $|J_\perp| \approx |J_y|$ toward the flanks (in the case of predominantly northward or southward IMF when the current system is expected to be located approximately in the equatorial plane). Figure 7 shows $|J_y|$ versus Y for three different clock angle ranges, predominantly northward IMF ($0° \le |\theta| \le 50°$, circles), predominantly southward IMF ($130° \le |\theta| \le 180°$ triangles), and intermediate clock angles ($50° \le |\theta| \le 130°$, crosses). From the figure, we see no clear tendency of $|J_y|$ decreasing toward large $|Y|$ when IMF $|B_z|$ is large, that is, for IMF configurations for which we expect that the current closure is in the equatorial plane. This may indicate that the major location of current closure is located further tailward, that is, beyond the MMS probing region.

4. Summary and Discussion

An electric current in the plane of the bow shock, $J_\perp$, is required for the pileup of the IMF in the magnetosheath. This current would not close locally, since then the magnetic pileup cannot be maintained globally. Instead, numerical simulations and theoretical arguments have predicted that $J_\perp$ must close across the magnetosheath to the magnetospheric current systems where the energy eventually is dissipated (e.g., Lopez et al., 2011; Siebert and Siscoe, 2002). At least close the bow shock, on the magnetosheath side, such a closure should manifest itself by the existence of a current component, J_n, approximately parallel or antiparallel to the bow shock normal, that is, a current on the average oriented toward $J_\perp$ on one side of the nonmidnight meridian, and away from $J_\perp$ on the other side, to create a closed-like current system (cf. Figure 1a) for the case with a southward IMF.

In this article we have used 2 years of dayside MMS data to observationally investigate the current systems, and any possible signatures of current closure, associated with quasi-perpendicular bow shocks of generator type, $\mathbf{E} \cdot \mathbf{J} < 0$. In total we have studied 154 clear MMS bow shock crossings distributed over GSM $-6.8 R_E < Y < 8.6 R_E$ and with upstream IMF clock angles in the range $2° < |\theta| < 180°$. The events are in general observed more toward positive Y, since quasi-perpendicular bow shocks are more common on the duskside due to the overall Parker spiral configuration of the IMF. The MMS mission is in a low-inclination orbit. Therefore, we have only studied the current systems near the equatorial plane.

It is known that the bow shock responds to variations in the upstream solar wind, for example, by moving sunward or Earthward (e.g., Maksimovic et al., 2003). But also during rather stable conditions, it can be both nonuniform and nonstationary. For example, ripples can propagate on the surface and it has been suggested that the shock can exhibit cyclical reformation (e.g., Auer et al., 1962; Eastwood et al., 2005; Johlander et al., 2016). As shown in section 3, the events included in our database are observed Earthward of the nominal subsolar position of the bow shock, indicating that they correspond to rather elevated upstream solar wind conditions. Moreover, it is likely that our events exhibit some kind of nonstationarity even though only the most clean ones have been selected for our study. However, even though our events do not correspond to standard solar wind conditions, we do not expect this to cause any qualitative effects on our results. The magnitude of the observed currents may change for disturbed solar wind conditions, but there should be no

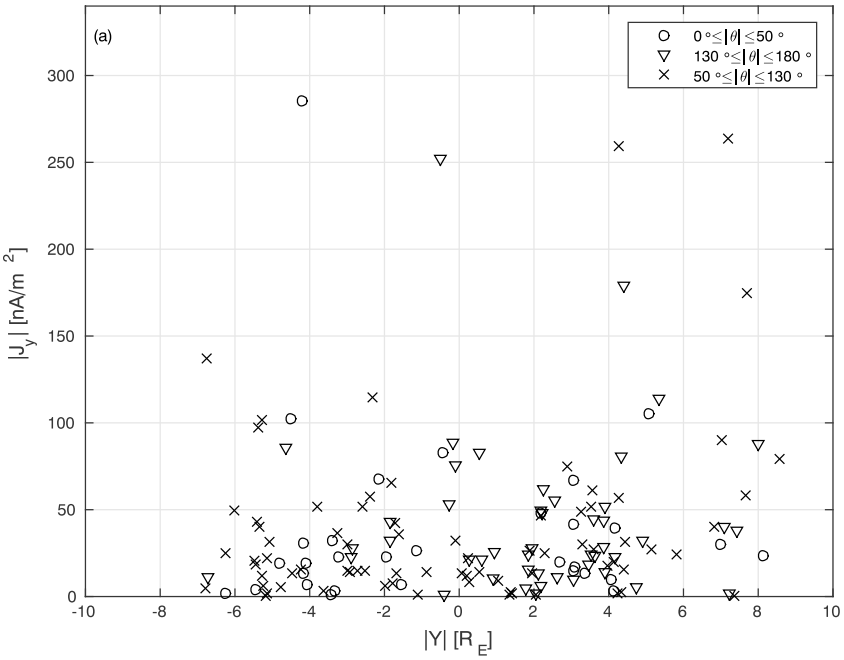

Figure 7. GSM $|J_y|$ versus Y in the clock angle ranges $0° \le |\theta| \le 50°$ (circles), $130° \le |\theta| \le 180°$ (triangles), and $50° \le |\theta| \le 130°$ (crosses).

effects on the large-scale current closure. For example, to decelerate an incoming fast solar wind at the bow shock, the $\mathbf{J} \times \mathbf{B}$ force must be large. This can be caused by either a strong $\mathbf{J}$ or a large $\mathbf{B}$, or both. However, the direction of the bow shock current will still be the same (for the same IMF direction), independent of the solar wind speed, and the conclusions of this article are the same.

The MMS spacecraft are equipped with magnetometers with unprecedented accuracy and interspacecraft calibration. Moreover, our events are selected to correspond to clear bow shock crossing with as little disturbances as possible, and with spacecraft configurations close to equilateral (see section 2). The curlometer should therefore be able to resolve the current density, at least near the shock ramp where there are clear magnetic field signatures, and with a resolution determined by the survey mode sampling frequency (16 s^{-1}) (Dunlop & Eastwood, 2008). In our investigation we have hence used the curlometer for estimating the current density, but whenever possible we have compared and verified the result (not shown) with the current density obtained from burst data ion and electron moments for those events where such data are available (see, e.g., Graham et al., 2016, for an example of the procedure).

We find that we can accurately capture $J_\perp$ in the plane of the bow shock and that it is consistently directed westward (eastward) for a southward (northward) component of the IMF. The confirmation of the expected current system verifies the use of the curlometer for our events, as does the behavior of the $\mathbf{F} = \mathbf{J} \times \mathbf{B}$ force, with F_x and F_y consistently oriented so that they decelerate the incoming solar wind flow and deviates it around the magnetosphere.

The observed $|J_n|$ is significantly weaker than $|J_\perp|$, and we suggest that the reason for this is that J_n is distributed over large regions and/or the MMS spacecraft do not exactly probe the main region of current closure where the currents are strongest. For cases with a predominantly southward IMF (i.e., $B_z < 0$, large IMF clock angles $|\theta|$), we find that J_n is oriented toward (away from) the westward $J_\perp$ on the duskside (dawnside) of $Y \sim 0$. Similarly, for cases with a predominantly northward IMF ($B_z > 0$, small clock angles $|\theta|$) , we obtain the same pattern but with the direction of all currents reversed. This is consistent with the simple pictured suggested by, for example, Siebert and Siscoe (2002) and Lopez et al. (2011) where the bow shock $J_\perp$ closes across the magnetosheath. To our knowledge, our results present the first observational evidence of such a current closure.

However, any global currents closing through the interior of the magnetosheath are much more difficult to resolve with observed data than the currents $J_\perp$ and $|J_n|$ near the bow shock. There are several reasons for this. For example, such global magnetosheath currents must be much smaller than the currents in the plane of the bow shock (since they are expected to be distributed over large spatial regions), and there are various disturbances in the magnetosheath proper making the magnetic field variation between the spacecraft far from linear (making the curlometer method not optimal for computing the current density). Instead of attempting to measure any global magnetosheath currents, in this article we focus on measuring the normal current component, J_n, close to the bow shock where the curlometer is expected to be reliable. The resulting picture we obtain from the separate events and from our statistical study in section 3 is fully consistent with theoretical arguments and numerical predictions. This verifies the validity of the results and the choice of methods for our investigation.

As a consequence of current continuity, and for the case of a predominantly northward or southward IMF (i.e., when the current system is expected to be located in the equatorial plane), $|J_\perp|$ should decrease toward the dusk and dawn flanks as more and more of the current is diverted toward the magnetosphere in the form of $|J_n|$. However, we observe no clear decrease of $|J_\perp|$ toward large $|Y|$ in our data, and we hence conclude that the main region of current closure must be further tailward, that is, outside the region where MMS was probing.

It is likely that the bow shock current system obtains a significant $J_{\perp z}$ component and that it hence is tilted away from the *xy* plane, when there is a significant IMF $|B_y|$ component. Indeed, in this article we show that the simple picture of J_n being oppositely directed on the duskside and dawnward side of $Y \sim 0$ works best for the smallest and largest clock angles but not for clock angles rather close to 90°. For angles in the intermediate range of approximately $50° \leq |\theta| \leq 130°$, no such signatures are seen in the data in the equatorial plane. Instead, for angles ~90° we see indications of increasing contributions from $E_z J_z$ to the total power density, while the contributions from $E_y J_y$ decrease. We therefore suggest that the bow shock current system is tilted toward the north-south direction when the IMF has a significant east-west component and that the closure of the bow shock current occurs off the equatorial plane and toward higher latitudes where the MMS spacecraft are not probing.

The utility of circuit analogs and electric currents for analyzing and understanding space physics processes has been discussed over the years. For example, it has been argued that electric circuit analogs cannot be used to predict the behavior of space plasmas and that the physics is better described by the magnetic field and the velocity (the B-V paradigm) than the electric field and the current density (the E-J paradigm) (e.g., Parker, 1996, 2000; Vasyliūnas, 2001). However, Parker (1996, 2000) also noted that a circuit language can still be adopted at a later stage after the magnetic field and velocity have been consistently obtained (e.g., from MHD simulations or observations). It should indeed be noted that the concept of electric currents has proven to be practical in many cases, since it helps us analyze and understand important processes such as the transport of energy and momentum in a system. For example, currents and electric fields have been useful when studying processes in the auroral region (e.g., Paschmann et al., 2002). The usefulness of circuit analogs and the relation to the MHD description were discussed quite extensively by Siebert and Siscoe (2002). They pointed out that circuit analogs are essential when trying to understand the role of the bow shock in the solar wind-magnetosphere system and what are driving the magnetopause reconnection loads.

There has not been much discussion in the literature about where the bow shock current should close across the magnetosheath. Is the closure located more toward the dayside as inferred from the simulations of Siebert and Siscoe (2002) and Lopez et al. (2011)? Or is it located further tailward as implied by the simulations of Guo et al. (2008) and Tang et al. (2009)? At what latitudes is it connecting toward the magnetospheric currents? It is possible that there is not a single answer to these questions. Instead, it is likely that the location of the closure varies with, for example, varying solar wind and IMF conditions and with variations in the magnetospheric current systems and loads. For example, for a predominantly southward (northward) IMF B_z, the magnetopause reconnection load is expected to exist near the subsolar point (tailward of the cusps), and it can be displaced azimuthally when there is a significant IMF $|B_y|$ (e.g., Laitinen et al., 2007). However, there is yet no simple model that describes when and where the bow shock current closes to the magnetospheric current systems. Moreover, a better understanding of the coupled solar wind-magnetospheric system is needed, for example, when investigating the magnetospheric energy budget and when investigating space weather effects.

Acknowledgments
M. H. was supported by the Swedish National Space Board (SNSB) grants 77/14, 271/14, 105/14, and 201/15, H. G. by the Belgian Science Policy Office through the Solar Terrestrial Centre of Excellence, and J. L. by the SNSB grant 201/15. We thank the MMS Science Data Center and all the MMS teams, especially the magnetic field, electric field, and the ion teams, in producing high-quality data. We are also grateful to the OMNIWeb and SPDF staff for providing high-quality solar wind data. All data are available through https://lasp.colorado.edu/mms/sdc/public/ and https://omniweb.gsfc.nasa.gov/. We thank P. Norqvist and A. De Spiegeleer for fruitful discussions.

References

Anekallu, C. R., Palmroth, M., Koskinen, H. E. J., Lucek, E., & Dandouras, I. (2013). Spatial variation of energy conversion at the Earth's magnetopause: Statistics from Cluster observations. *Journal of Geophysical Research: Space Physics*, *118*, 1948–1959. https://doi.org/10.1002/jgra.50233

Auer, P. L., Hurwitz, H., & Kilb Jr., R. W. (1962). Large-amplitude magnetic compression of a collision-free plasma. II. Development of a thermalized plasma. *Physics of Fluids*, *5*, 298–316. https://doi.org/10.1063/1.1706615

Bale, S. D., Balikhin, M. A., Horbury, T. S., Krasnoselskikh, V. V., Kucharek, H., Möbius, E., … Thomsen, M. F. (2005). Quasi-perpendicular shock structure and processes. *Space Science Reviews*, *118*, 161–203. https://doi.org/10.1007/s11214-005-3827-0

Burch, J. L., Moore, T. E., Torbert, R. B., & Giles, B. L. (2015). Magnetospheric multiscale overview and science objectives. *Space Science Reviews*, *199*, 5–21. https://doi.org/10.1007/s11214-015-0164-9

Burgess, D., Lucek, E. A., Scholer, M., Bale, S. D., Balikhin, M. A., Balogh, A., … Walker, S. N. (2005). Quasi-parallel shock structure and processes. *Space Science Reviews*, *118*, 205–222. https://doi.org/10.1007/s11214-005-3832-3

Burgess, D., Möbius, E., & Scholer, M. (2012). Ion acceleration at the Earth's bow shock. *Space Science Reviews*, *173*, 5–47. https://doi.org/10.1007/s11214-012-9901-5

Dmitriev, A., Chao, J., & Wu, D. (2003). Comparative study of bow shock models using Wind and Geotail observations. *Journal of Geophysical Research*, *108*(A12), 1464. https://doi.org/10.1029/2003JA010027

Dunlop, M. W., & Eastwood, J. P. (2008). The curlometer and other gradient based methods. *ISSI Scientific Reports Series*, *8*, 17–26.

Eastwood, J. P., Lucek, E. A., Mazelle, C., Meziane, K., Narita, Y., Pickett, J., & Treumann, R. A. (2005). The foreshock. *Space Science Reviews*, *118*, 41–94. https://doi.org/10.1007/ s11214-005-3824-3

Ergun, R. E., Tucker, S., Westfall, J., Goodrich, K. A., Malaspina, D. M., Summers, D., … Cully, C. M. (2016). The axial double probe and fields signal processing for the MMS mission. *Space Science Reviews*, *199*, 167–188. https://doi.org/10.1007/s11214-014-0115-x

Farris, M. H., & Russell, C. T. (1994). Determining the standoff distance of the bow shock: Mach number dependence and use of models. *Journal of Geophysical Research*, *99*, 17,681–17,689. https://doi.org/10.1029/94JA01020

Fedder, J. A., Slinker, S. P., Lyon, J. G., Russell, C. T., Fenrich, F. R., & Luhmann, J. G. (1997). A first comparison of POLAR magnetic field measurements and magnetohydrodynamic simulation results for field-aligned currents. *Geophysical Research Letters*, *24*, 2491–2494. https://doi.org/10.1029/97GL02608

Graham, D. B., Khotyaintsev, Y. V., Norgren, C., Vaivads, A., André, M., Lindqvist, P.-A., … Burch, J. L. (2016). Electron currents and heating in the ion diffusion region of asymmetric reconnection. *Geophysical Research Letters*, *43*, 4691–4700. https://doi.org/10.1002/2016GL068613

Guo, X. C., Wang, C., Hu, Y. Q., & Kan, J. R. (2008). Bow shock contributions to region 1 field-aligned current: A new result from global MHD simulations. *Geophysical Research Letters*, *35*, L03108. https://doi.org/10.1029/2007GL032713

Hamrin, M., Marghitu, O., Norqvist, P., Buchert, S., André, M., Klecker, B., … Dandouras, I. (2011). Energy conversion regions as observed by Cluster in the plasma sheet. *Journal of Geophysical Research*, *116*, A00K08. https://doi.org/10.1029/2010JA016383

Hamrin, M., Marghitu, O., Norqvist, P., Buchert, S., André, M., Klecker, B., … Dandouras, I. (2012). The role of the inner tail to midtail plasma sheet in channeling solar wind power to the ionosphere. *Journal of Geophysical Research*, *117*, A06310. https://doi.org/10.1029/2012JA017707

Hamrin, M., Marghitu, O., Rönnmark, K., Klecker, B., André, M., Buchert, S., … Vaivads, A. (2006). Observations of concentrated generator regions in the nightside magnetosphere by Cluster/FAST conjunctions. *Annales Geophysicae*, *24*, 637–649. https://doi.org/10.5194/angeo-24-637-2006

Ieda, A., Fairfield, D. H., Mukai, T., Saito, Y., Kokubun, S., Liou, K., … Brittnacher, M. J. (2001). Plasmoid ejection and auroral brightenings. *Journal of Geophysical Research*, *106*, 3845–3858. https://doi.org/10.1029/1999JA000451

Johlander, A., Schwartz, S. J., Vaivads, A., Khotyaintsev, Y. V., Gingell, I., Peng, I. B., … Burch, J. L. (2016). Rippled quasiperpendicular shock observed by the magnetospheric multiscale spacecraft. *Physical Review Letters*, *117*(16), 165101. https://doi.org/10.1103/PhysRevLett.117.165101

Laitinen, T. V., Palmroth, M., Pulkkinen, T. I., Janhunen, P., & Koskinen, H. E. J. (2007). Continuous reconnection line and pressure-dependent energy conversion on the magnetopause in a global MHD model. *Journal of Geophysical Research*, *112*, A11201. https://doi.org/10.1029/2007JA012352

Lindqvist, P.-A., Olsson, G., Torbert, R. B., King, B., Granoff, M., Rau, D., … Tucker, S. (2016). The spin-plane double probe electric field instrument for MMS. *Space Science Reviews*, *199*, 137–165. https://doi.org/10.1007/s11214-014-0116-9

Lopez, R. E., Merkin, V. G., & Lyon, J. G. (2011). The role of the bow shock in solar wind-magnetosphere coupling. *Annales Geophysicae*, *29*, 1129–1135. https://doi.org/10.5194/angeo-29-1129-2011

Maksimovic, M., Bale, S. D., Horbury, T. S., & André, M. (2003). Bow shock motions observed with CLUSTER. *Geophysical Research Letters*, *30*, 1393. https://doi.org/10.1029/2002GL016761

Marghitu, O., Hamrin, M., Klecker, B., Vaivads, A., McFadden, J., & Buchert, S. (2006). Experimental investigation of auroral generator regions with conjugate Cluster and FAST data. *Annales Geophysicae*, *24*, 619–635. https://doi.org/10.5194/angeo-24-619-2006

Merka, J., Szabo, A., Šafránková, J., & Němeček, Z. (2003). Earth's bow shock and magnetopause in the case of a field-aligned upstream flow: Observation and model comparison. *Journal of Geophysical Research*, *108*, 1269. https://doi.org/10.1029/2002JA009697

Parker, E. N. (1996). The alternative paradigm for magnetospheric physics. *Journal of Geophysical Research*, *101*, 10,587–10,626. https://doi.org/10.1029/95JA02866

Parker, E. N. (2000). *Newton, Maxwell, and magnetospheric physics, Geophysical Monograph Series* (Vol. 118, 1 pp.). Washington, DC: American Geophysical Union. https://doi.org/10.1029/GM118p0001

Paschmann, G., Haaland, S., & Treumann, R. (2002). Auroral Plasma Physics. *Space Science Reviews*, *103*(1–4), 41–92. https://doi.org/10.1023/A:1023030716698

Paschmann, G., & Schwartz, S. J. (2000). ISSI book on analysis methods for multi-spacecraft data. In R. A. Harris (Ed.), *Proceedings of the Cluster-II Workshop Multiscale / Multipoint Plasma Measurements* (Vol. 449, 99 pp.). London, UK: ESA Special Publication.

Pollock, C., Moore, T., Jacques, A., Burch, J., Gliese, U., Saito, Y., … Zeuch, M. (2016). Fast plasma investigation for magnetospheric multiscale. *Space Science Reviews*, *199*, 331–406. https://doi.org/10.1007/s11214-016-0245-4

Rosenqvist, L., Buchert, S., Opgenoorth, H., Vaivads, A., & Lu, G. (2006). Magnetospheric energy budget during huge geomagnetic activity using Cluster and ground-based data. *Journal of Geophysical Research*, *111*, A10211. https://doi.org/10.1029/2006JA011608

Rosenqvist, L., Opgenoorth, H. J., Rastaetter, L., Vaivads, A., Dandouras, I., & Buchert, S. (2008). Comparison of local energy conversion estimates from Cluster with global MHD simulations. *Geophysical Research Letters*, *35*, L21104. https://doi.org/10.1029/2008GL035854

Rosenqvist, L., Vaivads, A., Retinò, A., Phan, T., Opgenoorth, H. J., Dandouras, I., & Buchert, S. (2008). Modulated reconnection rate and energy conversion at the magnetopause under steady IMF conditions. *Geophysical Research Letters*, *35*, L08104. https://doi.org/10.1029/2007GL032868

Russell, C. T. (1985). Planetary bow shocks. In B. T. Tsurutani, & R. G. Stone (Eds.), *Collisionless shocks in the heliosphere: Reviews of current research, Geophysical Monograph Series* (Vol. 35, pp. 109–130). Washington DC: American Geophysical Union. https://doi.org/10.1029/GM035p0109

Russell, C. T., Anderson, B. J., Baumjohann, W., Bromund, K. R., Dearborn, D., Fischer, D., … Richter, I. (2014). The magnetospheric multiscale magnetometers. *Space Science Reviews*, *199*, 189–256. https://doi.org/10.1007/s11214-014-0057-3

Samsonov, A. (2006). Numerical modelling of the Earth's magnetosheath for different IMF orientations. *Advances Space Research*, *38*, 1652–1656. https://doi.org/10.1016/j.asr.2005.06.009

Siebert, K. D., & Siscoe, G. L. (2002). Dynamo circuits for magnetopause reconnection. *Journal of Geophysical Research*, *107*, 1095. https://doi.org/10.1029/2001JA000237

Siscoe, G. L., & Cummings, W. D. (1969). On the cause of geomagnetic bays. *Planetary and Space Science*, *17*, 1795–1802. https://doi.org/10.1016/0032-0633(69)90055-5

Siscoe, G. L., & Siebert, K. D. (2006). Bimodal nature of solar wind magnetosphere ionosphere thermosphere coupling. *Journal of Atmospheric and Solar-Terrestrial Physics*, *68*, 911–920. https://doi.org/10.1016/j.jastp.2005.11.012

Slavin, J. A., Smith, M. F., Mazur, E. L., Baker, D. N., Hones, E. W., Iyemori Jr., T., & Greenstadt, E. W. (1993). ISEE 3 observations of traveling compression regions in the Earth's magnetotail. *Journal of Geophysical Research*, *98*(15), 15,425–15,446. https://doi.org/10.1029/93JA01467

Tang, B. B., Guo, X. C., Wang, C., Hu, Y. Q., & Kan, J. R. (2009). Bow shock and magnetopause contributions to the cross-tail current from global MHD simulations. *Journal of Geophysical Research*, *114*, A08203. https://doi.org/10.1029/2009JA014325

Tang, B. B., Wang, C., & Guo, X. C. (2012). Bow shock and magnetopause contributions to the magnetospheric current system: Hints from the Cluster observations. *Journal of Geophysical Research*, *117*, A01214. https://doi.org/10.1029/2011JA016681

Torbert, R. B., Russell, C. T., Magnes, W., Ergun, R. E., Lindqvist, P.-A., LeContel, O., … Lappalainen, K. (2014). The FIELDS instrument suite on MMS: Scientific objectives, measurements, and data products. *Space Science Reviews*, *199*(1–4), 105–135. https://doi.org/10.1007/s11214-014-0109-8

Vasyliūnas, V. M. (2001). Electric field and plasma flow: What drives what? *Geophysical Research Letters*, *28*, 2177–2180. https://doi.org/10.1029/2001GL013014